Final Report

Contract No. N00014-91-J-1635

Intrinsic, P-doped and modulation-doped quantum well Lasers for ultrafast modulation and ultrashort pulses

Issued by

Office of Naval Research

to

University of California at Berkeley
Department of Electrical Engineering and Computer Science

Principal Investigator

K.Y. Lau

Contract Period: 4/1/91 - 2/28/92

1. Introduction

During the course of this contract, we studied experimentally and theoretically the fundamental limit in the modulation bandwidth of quantum well lasers. The motivation of this study arises from the fact that. despite numerous predictions in the last few years on the potential superiority of quantum well lasers in high speed modulation, none of them have been successfully verified experimentally. The initial approach was to study gain compression as a fundamental mechanism of limiting modulation bandwidths of quantum well lasers. To the extent that the physics behind gain compression was not known, a major effort was put in uncovering the fundamental physics responsible for gain compression. It was subsequently discovered that the finite carrier capture time into the quantum well, despite being a very fast process (1ps or less), can lead to a large gain compression parameter. We have then proceeded along this line and studied the fundamental quantum capture of electrons and holes into quantum wells, as well as the consequence of these capture processes in the modulation dynamics of quantum well lasers. The goal here is not only to understand *what limits the modulation* bandwidth of quantum well lasers, but to make use of that knowledge to design suitable structures for overcoming these limitations. The following sections contain detailed descriptions of the experimental and theoretical work that uncovered the above facts.

2. Transport in quantum well lasers - a fundamental limitation in high speed modulation

Quantum well lasers, in particular strained quantum well lasers, are expected to possess very large modulation bandwidths, owing to a large differential gain. On the other hand, if these large differential gains are inevitably accompanied by a large gain compression, then the predicted advantages could largely be negated [Sharfin 1991]. Whether this is true or not depends on the physical origin of gain compression. As mentioned before, a number of such mechanisms have been proposed for the origin of gain compression, including spectral hole-burning and carrier heating. Both of these effects are intrinsically present in any semiconductor lasers and will definitely contribute to gain compression, but the question is whether they yield numerical values and trends consistent with experimental observations. To the date of this writing, it appears that these mechanisms generally give gain compression values too small compared to experiments, and the dependence on various laser parameters, such as device length and threshold density, are not consistent with observations either. These imply that some other physical mechanisms are present in quantum well lasers that dominate over the above mechanisms. A new model (the "reservoir" model) recently proposed by Rideout et al. [Rideout 1991] considered the consequence of a small but finite capture and escape time of the carriers between the separate confinement (SCH) region and the quantum well(s). These time constants are in the picosecond time scale and have in the past been considered too small to be of any consequence in the direct modulation response of injection laser up to 100GHz. What Rideout et al. proposed, however, was that these small time constants contribute, in principle, significantly to the gain compression parameter. Furthermore, the model predicts a linear scaling relationship between the gain compression coefficient (ϵ) and differential gain (dg/dn), with the proportionality constant depending on these small transport times. If this model were correct there will exist an ultimate limit in the modulation bandwidth of quantum well lasers despite a high differential gain in these lasers.

While the carrier capture and escape time constants used in the original "reservoir" model

was described only phenomenologically, Nagarajan et al. [Nagarajan 1991] attributed carrier diffusion across the SCH region as being a major contributor to the capture time, and classical thermionic emission as the major physical mechanism for carrier escape from the quantum well, as supported by experimental results from quantum well lasers with various SCH widths [Nagarajan 1991]. Futhermore, when one considers the rate equations involved in the transport in more detail, it was found that the effect of transport is more than just an increase gain compression - it has other consequences in terms of modifying the relaxation oscillation frequency and the shape of the response function[Nagarajan 1991][Wu 1992]. We shall consider some of issues in this section.

The "reservoir" model is illustrated schematically in Fig. 1. The confined electrons (in the quantum well) and the unconfined electrons in the SCH region are represented by distinct reservoirs. The exchange of carriers between these two reservoirs are described by time constants, τ_{cap} and τ_{esc}, for the capture and escape processes, respectively. The capture and escape processes are intrinsically described by phonon-assisted quantum transitions, but for lasers with a very wide SCH region, the capture time has been attributed primarily as due to classical carrier diffusion in the SCH region[Nagarajan 1991]. Rate equations can then be written that describe exchange of carriers between the reservoirs of unconfined and confined carriers, and between the latter and the lasing photons. The small signal rate equations are [Rideout 1991]:

$$\frac{ds}{dt} = \Gamma G' S_o n_a \tag{1}$$

$$\frac{dn_2}{dt} = (\frac{n_3}{\tau_{cap}} - \frac{n_2}{\tau_{esc}}) - G' S_o n_a - \frac{s}{\Gamma \tau_p} - \frac{n_2}{\tau_2} \tag{2}$$

$$\frac{dn_3}{dt} = -(\frac{n_3}{\tau_{cap}} - \frac{n_2}{\tau_{esc}}) + j_{pump} - \frac{n_3}{\tau_3} \tag{3}$$

where s, n_2, and n_3 are the (small signal) photon density, carrier density in the confined quantized states, and carrier density in the unconfined states in the SCH regions (reservoir), respectively, Γ is the confinement factor, $G' = vdg/dn_a \equiv vg'$, S_o is the photon density at the bias point, τ_2 and τ_3 are the recombination times, τ_p is the photon lifetime, and j_{pump} is the pumping current

density. As in [Rideout 1991], no gain compression coefficient is explicitly incorporated into the above equations. The effective gain compression coefficient ϵ_{cap} deduced from these equations is purely due to the carrier capture effect. The total ϵ is then the sum of the effective ϵ_{cap} and ϵ_{other}, where ϵ_{other} is due to other mechanisms such as spectral hole burning [Takahashi 1991], carrier heating [Kesler 1987] and standing wave effect [Su 1988].

The response function s/j_{pump} in this model was considered by Rideout et al. [Rideout 1991]. In the following, this response function will be studied using series expansion. The recombination terms in equations (2) and (3) are neglected for simplicity as the recombination times (τ_2 and τ_3) are typically a few nanoseconds, and therefore larger than the time scale of interest. From equation (3), we obtained an expression for net capture current as:

$$\frac{n_3}{\tau_{cap}} - \frac{n_2}{\tau_{esc}} = \frac{n_2}{\tau_{esc}}\left(\frac{-i\omega\tau_{cap}}{1+i\omega\tau_{cap}}\right) + \frac{j_{pump}}{1+i\omega\tau_{cap}} \tag{4}$$

Following a standard analysis on the rate equations (1) and (2), we obtain the modulation response:

$$\frac{s}{j_{pump}} = \frac{\Gamma G' S_o}{-\omega^2(1+R+i\omega\tau_{cap}) + (1+i\omega\tau_{cap})(i\omega G' S_o + \omega_r^2)} \equiv \frac{\Gamma G' S_o}{F(\omega)} \tag{5}$$

where $\omega_r = \sqrt{G' S_o/\tau_p}$ (the conventional relaxation oscillation frequency) and $R = \tau_{cap}/\tau_{esc}$. In the limit of extremely small capture time ($\omega\tau_{cap} \to 0$), $F(\omega) \to F^{(0)}(\omega)$:

$$F^{(0)}(\omega) = -\omega^2(1+R) + i\omega G' S_o + \omega_r^2 \tag{6}$$

This expression differs from the conventional modulation response [Rideout 1991] in that the inertia of the relaxation oscillation is increased by the factor 1+R, resulting in a lowering of the relaxation oscillation frequency and the damping rate by the same factor [Nagarajan 1991][Wu 1992]. Note that the modification of the resonant oscillation inertia depends only on the ratio $R = \tau_{cap}/\tau_{esc}$ and not on the absolute values of τ_{cap} or τ_{esc}.

In the limit of small but finite τ_{cap} ($\omega\tau_{cap} \ll 1$), the denominator of the modulation response can be factorized as:

$$F(\omega) \approx F^{(1)}(\omega) = \left(1 - \frac{\omega}{\omega_3}\right)\left\{-\omega^2(1+R) + i\omega G' S_o\left[1 + \tau_{cap}\frac{R}{1+R}\left(\frac{1}{\tau_p}\right)\right] + \widetilde{\omega_r}^2\right\} \tag{7}$$

where $\widetilde{\omega_r}^2 = \omega_r^2[1 - \tau_{cap}R/(1+R)^2 G' S_o]$ and $1/\omega_3 \approx -i\tau_{cap}/(1+R)$. A corresponding $F(\omega)$ can be obtained using a differential gain constant $G'_o(1-\epsilon S)$ in the conventional rate equations [Tucker 1985]:

$$F(\omega) = -\omega^2 + i\omega G'_o S_o\Big[1 + \frac{\epsilon}{G'_o}(\frac{1}{\tau_p})\Big] + \omega_r^2 \tag{8}$$

By comparing equation (7) and (8) and neglecting the pole at $\omega = \omega_3$ in equation (7), it is observed that the carrier capture effect is equivalent to a gain compression effect. However, one has to be very careful in making the comparison because the factor 1+R in ω^2 term in equation (7) reduces the damping rate (the coefficient of $i\omega$ term) as well as the resonance frequency. The effective ϵ_{cap} due to the carrier capture time effect can then be expressed as:

$$\epsilon_{cap} = \tau_{cap}\frac{R}{1+R}G'_o = \tau_{cap}\frac{R}{1+R}v(g')_{eff} \tag{9}$$

where $(g')_{eff} = (g')/(1+R)$ is the effective differential gain. Note that our expression for ϵ_{cap} differs from the result in [Rideout 1991] by an additional factor of 1+R. The quantity $(g')_{eff}$ can be deduced experimentally from the observed resonant frequency ω_r^{ex} as: $(g')_{eff} = (\omega_r^{ex2}/S_o)(\tau_p/v)$.

The linear dependence between ϵ and g' has been experimentally observed recently[Wu 1992]. The laser used was a tensile strained $1.55\mu m$ quantum well laser with the following structure: a 200 $\AA$ thick $In_{0.41}Ga_{0.59}As$ single quantum well is sandwiched by SCH layers as shown in the inset of Fig.2. Lateral confinement is provided by a 1.5 μm wide waveguide buried with semi-insulating InP. The lasers are then cleaved into different cavity lengths with a one-sided HR coating applied on some of the devices. The setup for measuring the modulation response of the lasers is an optical modulation method similar to that reported previously [Lange 1989]. The laser used for modulation injection is a 1.3 μm diode laser with the 3dB bandwidth of 10 GHz, at approximately 10 mW output power. The measurement results are summarized in Table I. For both sets of HR coated and uncoated samples, the internal quantum efficiency and internal loss are determined to be around 47% and 2.62 cm^{-1}, respectively. The differential gain and the gain compression coefficient (ϵ) are determined from the measured slopes of relaxation oscillation

frequency squared versus power and the measured K factor [Bowers 1987]. The resulting values are also listed in Table I.

One notices from Table I that samples (1) to (3) lase in the first quantized state while samples (4) to (7) lase in the second quantized state; as is evident from the lasing wavelengths, which are separated by 56 meV (corresponding to a 200 $\AA$ well) between the two sets of samples. Fig.2 plots g' versus threshold gain. The solid circles indicate lasing in the first quantized state, while the crosses denote lasing in the second quantized state. The transition takes place at a threshold gain of around 20 cm^{-1}. Note the abrupt increase in g' at the transition to second quantized state lasing and the subsequent decrease in g' at very high gain. This variation of g' with threshold gain is consistent with a standard model of quantum well gain [Mittelstein 1986]. The linear dependence of the gain compression coefficient ϵ on dg/dn can be visualized by plotting the ratio $\epsilon/(v_g dg/dn)$, which is the K-factor less the part involving photon lifetime (i.e., $K' = K - 4\pi^2\tau_p$), versus threshold gain as shown in Fig.3. The factor v is the group velocity of light. These experimental results show that K' is basically constant to within $\pm 15\%$, despite the variation in g' by a factor of two among the samples.

As discussed above, the total $\epsilon = \epsilon_{cap} + \epsilon_{other}$ is the sum of contributions from carrier capture effect ϵ_{cap} and other mechanisms ϵ_{other}. According to equation (22), the proportionality constant between ϵ_{cap} and $(g')_{eff}$, defined as B, is $v_g\tau_{cap}R/(1+R)$. In Fig.4, ϵ is plotted against $(g')_{eff}$ using the experimental results in Table I. The data are linearly fitted using a least square regression method. The y-intercept (ϵ_{other}) is $0.63 \times 10^{-17} cm^3$ and the slope of the line (B) is 0.087 cm. These data implies that $\tau_{cap} = 13ps$, assuming $v_g = 10^{10} cms^{-1}$ and R=2 [Rideout 1991]. This value of τ_{cap} is comparable to values measured independently in other experiments [Morin 1991]. The value of ϵ_{other} derived from our data is also comparable to the value derived from other mechanisms ([Takahashi 1991], [Kesler 1987], [Su 1988]). Dependency of ϵ on g' can also be obtained in the spectral hole burning theory for quantum well lasers. A recent calculation [Zhao 1992] illustrated this fact. However, the predicted value of the proportionality constant between ϵ and g' in [Zhao 1992] based on spectral hole burning is one order of magnitude smaller

than that observed experimentally. This implies that while spectral hole-burning produces gain-compression characteristics similar to that of the transport mechanism, the former may not be a dominant effect. As of this writing, intense effort is still underway to confirm or clarify these issues.

3. Quantum Capture and Escape in Quantum Well Lasers

As illustrated in the last section, carrier capture and escape processes play important roles in limiting the modulation bandwidth of quantum well lasers. Rideout et al. expressed the effect using an equivalent gain compression coefficient in the limit of short capture time. Nagarajan et al. considered theoretically the carrier diffusion in the separate confinement region and neglected the quantum capture effect. They showed experimentally that the relatively long capture time which causes the reduction of modulation bandwidth is predominantly due to carrier diffusion. However, regardless of the physical origins of the capture time, both formulations [Rideout 1991, Nagarajan 1991] are mathmatically equivalent with the result that the *capture* time constant (τ_{cap}) and the *ratio* of the *capture* to *escape* time constant ($R \equiv \tau_{cap}/\tau_{esc}$) are two important parameters which directly affect the modulation response. In particular, a large *ratio* R increases both the damping and inertia [Rideout 1991, Nagarajan 1991, Wu 1992] of the relaxation oscillation and is thus detrimental to high speed modulation. While the diffusion process is well-understood, the intrinsic quantum capture and escape rates have been dealt with only through phenomenological equivalent time constants. In order to have a clearer understanding of the relative importance of diffusion and the intrinsic quantum capture processes, it is necessary to consider the physical nature of the latter. It is well accepted that the dominant processes of transfering carriers into and out of III-V quantum well (QW) are via longitudinal optical (LO) phonon emission and absorption [Lester 1991, Blom 1990]. Based on these phonon-assisted processes, considerable effort has been undertaken (both theoretical and experimental) in establishing the rate of *capture* into the quantum well, while little attention was paid to the relative magnitude of *capture* and *escape* rates [Brum 1986]. Here, simple analytic expressions for the net carrier capture current are derived[Kan 1992a], which is then used to compute the *capture* and *escape* time constants (τ_{cap} and τ_{esc}) in an unified way and therefore, are able to calculate the *ratio* R under different operating conditions and for different QW structures.[Kan 1992a]

In quantum well structures, electronic states are classified into confined states $|c>=|E_z^c, \mathbf{k}_{//}^c>$ and unconfined states $|u>=|\mathbf{k}^u>$ where E_z^c is the longitudinal energy of the quantized state in quantum well, $\mathbf{k}^u = (k_z^u, \mathbf{k}_{//}^u)$ is the wavevector of unconfined state, $\mathbf{k}_{//}^c$ and $\mathbf{k}_{//}^u$ are the wavevectors parallel to the QW layers, and k_z^u is the wavevector perpendicular to the layers. Assuming transitions between $|c>$ and $|u>$ are LO phonon-assisted, an electron in $|u>$ is captured into $|c>$ by either emitting or absorbing a LO phonon as shown in Fig.5. An unconfined electron of energy E^u is scattered into the confined states of constant energy $E^c = E^u \pm E_{ph}$ on Ring-C. We assume a constant E_{ph} ($\sim$ 36 meV).

Let $w_1(\mathbf{k}^u)$ be the total departure rate for the electron from an unconfined state $|\mathbf{k}^u>$ to Ring-C by emitting one LO phonon:

$$w_1(\mathbf{k}^u) = \int_{Ring-C} r(u \rightarrow c)\, \rho(\mathbf{k}_{//}^c)\, d\mathbf{k}_{//}^c \tag{10}$$

where $r(u \rightarrow c)$ is the scattering rate from $|\mathbf{k}^u>$ to $|E_z^c, \mathbf{k}_{//}^c>$ with emission of one LO phonon and $\rho(\mathbf{k}_{//}^c)$ is the density of states. The total capture current density due to LO phonon emission may then be expressed as:

$$J_{cap}^{em} = 2\,(n_{ph}+1) \int_{-\infty}^{\infty} \frac{dk_z^u}{2\pi} \int_{-\infty}^{\infty}\int_{-\infty}^{\infty} \frac{d^2\mathbf{k}_{//}^u}{4\pi^2}\, w_1(\mathbf{k}^u)\, f^u(1-f^c) \tag{11}$$

where f^c and f^u are the Fermi-Dirac distributions for the confined and unconfined states, respectively, and n_{ph} is the phonon occupation number. If we assume the Fermi level is near or below the band edge of the barrier so that electrons are localized only in the states near $|\mathbf{k}^u| = 0$, we may neglect the $\mathbf{k}^u$ dependence in w_1. We then integrate over $\mathbf{k}_{//}^u$ in Eqn.11:

$$J_{cap}^{em} = n_o\,(n_{ph}+1)\, n_{ph}^-\, w_1 \int_0^{\infty} dk_z^u\, Log\Big\{\frac{1+exp[(E_f^c - E_z^u + E_{ph})/kT]}{1+exp[(E_f^u - E_z^u)/kT]}\Big\} \tag{12}$$

where E_f^c and E_f^u are the Fermi levels for the confined and unconfined states, respectively, $n_o = m^* kT/\pi^2\hbar^2$, m^* is the effective mass (the difference of m^* in different layers is neglected), and $n_{ph}^- = 1/\{\, exp[E_{ph}/kT]\, exp[-(E_f^u - E_f^c)/kT] - 1\,\}$. The top of the barrier is taken to be the zero energy reference and therefore, the longitudinal energy of unconfined state E_z^u equals

$(\hbar k_z^u)^2/2m^*$. The effective barrier height V_b in Fig.5 is the energy difference between the top of barrier and the first quantized state of the QW.

The reverse of the capture process is an escape process in which an electron on Ring-C jumps to $|\mathbf{k}^u>$ by absorbing a LO phonon. Because of the reversal symmetry of the scattering rate, $w_1(\mathbf{k}^u)$ is also the total arrival rate to $|\mathbf{k}^u>$ from the confined states on Ring-C. Similarly, we let $w_2(\mathbf{k}^u)$ be the total departure rate for the case of capture processes via phonon absorption. Again, because of the reversal symmetry of the scattering rate, $w_2(\mathbf{k}^u)$ is also the total arrival rate for escape processes via phonon emission. Using the same approach for J_{cap}^{em}, we obtain the expressions for J_{esc}^{ab}, J_{cap}^{ab}, and J_{esc}^{em},

$$J_{esc}^{ab} = n_o\,(n_{ph}^{+}+1)\,n_{ph}\,w_1\int_0^{\infty} dk_z^u\; Log\Big\{\frac{1+exp[(E_f^c-E_z^u+E_{ph})/kT]}{1+exp[(E_f^u-E_z^u)/kT]}\Big\} \tag{13}$$

$$J_{esc}^{em} = n_o\,(n_{ph}+1)\,n_{ph}^{+}\,w_2\int_0^{\infty} dk_z^u\; Log\Big\{\frac{1+exp[(E_f^u-E_z^u)/kT]}{1+exp[(E_f^c-E_z^u-E_{ph})/kT]}\Big\} \tag{14}$$

$$J_{cap}^{ab} = n_o\,(n_{ph}^{-}+1)\,n_{ph}\,w_2\int_0^{\infty} dk_z^u\; Log\Big\{\frac{1+exp[(E_f^u-E_z^u)/kT]}{1+exp[(E_f^c-E_z^u-E_{ph})/kT]}\Big\} \tag{15}$$

where $n_{ph}^{+} = 1/\{\,exp[E_{ph}/kT]\,exp[(E_f^u-E_f^c)/kT]\,-\,1\,\}$.

The total capture current ($J_{cap} = J_{cap}^{em} + J_{cap}^{ab}$), escape current ($J_{esc} = J_{esc}^{em} + J_{esc}^{ab}$), and net current ($J_{net} = J_{cap} - J_{esc}$) in a typical GaAs quantum well laser structure are calculated from Eqn.12-15 and plotted against $\Delta E_f \equiv E_f^u - E_f^c$ in Fig.6. Assuming $V_b \gg E_{ph}$, the Ring-C in Fig.5 for processes via phonon emission is very close to the Ring-C for processes via phonon absorption. Therefore, we take $w_1 \approx w_2 = w_o = 0.2ps^{-1}$ [Lester 1991, Blom 1990]. In a typical quantum well laser, the net current density J_{net}, which determines ΔE_f, is in the range of $100A/cm^2$ (near threshold operation) to $2000A/cm^2$ (high power operation). We have assumed only one quantized state exists in the QW. Existence of multiple quantized states will complicate the model due to the intersubband transitions and is currently under investigation. We consider the electron capture process only, assuming that the quantum capture of electrons is slower or the capture process is ambipolar [Morin 1991, Eisenstein 1991]. However, the same formulism can be applied in the study of hole capture.

Using Eqn.12-15, we calculate the *capture* time constant (τ_{cap}) and the *ratio* of the *capture* to *escape* time constant ($R \equiv \tau_{cap}/\tau_{esc}$) — the two determining parameters of the carrier capture effect on the modulation response, for different effective barrier heights (V_b) and carrier densities of confined states of quantum well (N_c) in the range of $J_{net} = 0$ to $2000A/cm^2$. The effective barrier height (V_b) is determined by the bandgap offset of QW and the quantum well width. The carrier density of confined states (N_c) is actually the threshold carrier density which is determined by the photon lifetime and number of QWs. The two time constants (τ_{cap} and τ_{esc}) are defined as $\tau_{cap} \equiv \partial J_{net}/\partial N_u$ and $\tau_{esc} \equiv \partial J_{net}/\partial N_c$, respectively, in the small signal rate equations of quantum well lasers [Wu 1992] where N_u is the carrier density of unconfined states. Note that τ_{cap} is determined by both the capture and escape currents since $J_{net} = J_{cap} - J_{esc}$. We assume w_o to be constant, independent of V_b, in this calculation. Recent calculations [Brum 1986] indicated that w_o oscillates with well thickness. However, such dependence has not been observed experimentally [Blom 1990]. *Nevertheless, our result for R is independent of w_o since* this factor is cancelled out. From our calculations, we find that when J_{net} is changed from 0 to 2000 A/cm^2, τ_{cap} and R are almost constant (within a few percent) even though J_{cap} is much larger than J_{esc} when J_{net} is large. This is illustrated in Fig.6 by plotting the *ratio* R versus ΔE_f. The average values of τ_{cap} and R over the range of $J_{net} = 0$ to $2000A/cm^2$ for lasers with different V_b and N_c are listed in Table II.

Simple analytic expressions for τ_{cap} and R can be obtained based on the fact that when R is comparable to or larger than unity, $(\Delta E_f)_{2000}$ is very small compared to kT. We then expand the expression for J_{net} to first order in $\Delta E_f/kT$:

$$J_{net} = \left(\frac{\Delta E_f}{kT}\right) J_o \int_0^\infty dk_z^u \, Log\left\{\frac{1 + exp[(E_f^c - E_z^u + E_{ph})/kT]}{1 + exp[(E_f^c - E_z^u - E_{ph})/kT]}\right\} \qquad (16)$$

where $J_o = n_o\, n_{ph}\, (n_{ph}+1)\, w_o$. The rate constants $1/\tau_{cap}$ and $1/\tau_{esc}$ can now be expressed as:

$$\begin{aligned}
\frac{1}{\tau_{cap}} &= \frac{1}{dN_u/dE_f^u}\, J_o\, \frac{1}{kT}\, I_{log} \\
\frac{1}{\tau_{esc}} &= \frac{1}{dN_c/dE_f^c}\, J_o\, \frac{1}{kT}\, [I_{log} - \frac{E_f^u - E_f^c}{kT} I_f] \\
&\approx \frac{1}{dN_c/dE_f^c}\, J_o\, \frac{1}{kT}\, I_{log} \qquad\qquad as \quad \Delta E_f \ll kT
\end{aligned} \tag{17}$$

where I_{log} is the integral in Eqn.16, $I_f = \int_0^\infty dk_z^u\ (f^+ - f^-)$, and $f^\pm = 1/\{exp[(\pm E_{ph} - E_f^c + E_z^u)/kT] + 1\}$. The *ratio* $R \equiv \tau_{cap}/\tau_{esc}$ then becomes:

$$R = (\frac{dN_u}{dE_f^u})/(\frac{dN_c}{dE_f^c}) \tag{18}$$

This factor is a function of carrier densities and densities of states of the confined and unconfined states, which depends on the QW structure. The dependence of R on the quantum well thickness is shown in Fig.7 for a quantum well laser operating at different threshold carrier densities (N_c). Note that the calculation for very wide quantum wells, which probably have a second quantized state, is for reference only since our model is valid only for wells with one quantized state. This is also the case for data in Table I for large V_b.

As discussed earlier, the gain compression coefficient of the laser increases with R and τ_{cap} and the relaxation oscillation frequency is reduced by a factor $1 + R$. The modulation response of quantum well lasers is thus degraded appreciably when $R \approx 1$. One notes from Table II that τ_{cap} is relatively constant with respect to the effective barrier height V_b and the carrier density of confined states N_c (which is the threshold carrier density of the laser), while the ratio R varies strongly with V_b and N_c. Furthermore, R is rather independent of the net injection current, as evident from Fig.6. The implications are as follows: (1) a multi-quantum well laser has a smaller R than a single quantum well laser due to the lower threshold *carrier* density of the former; (2) lasers with narrow or shallow QWs exhibit higher values of R due to a smaller effective barrier height V_b; (3) these effects are relatively independent of the bias current (and hence optical power). To completely understand the structural dependence of the modulation response, the effect of carrier diffusion in the separate confinement region of the device has to

be included. The calculations above consider the quantum capture effect only but can reveal dependences on device structure which are consistent with observed experimental results to date [Nagarajan 1991, Shimizu 1991, Uomi 1991], thus suggesting that quantum capture can play a significant role relative to the carrier diffusion effect.

4. Intrinsic Equivalent Circuit of Quantum Well Lasers

Intrinsic equivalent circuit of semiconductor lasers is useful not only for designing electronic circuitry with which the laser operates, but also for furthering the understanding of laser dynamics and noise properties [Katz 1981, Harder 1982c, Harder 1990]. The intrinsic equivalent circuit of a bulk semiconductor laser has been developed a decade ago [Katz 1981, Harder 1982c]. Similar approaches was applied to quantum well lasers [Harder 1990]. However, with the recent understanding of the importance of transport in quantum well lasers as described in the last two sections, it becomes necessary to revise the well-accepted equivalent circuit models to include these effects [Kan 1992b]. It is assumed here that the SCH region in the laser structure is sufficiently narrow so that carrier diffusion is not a significant factor [Nagarajan 1991]. Using this circuit model, certain qualitative features of the modulation dynamics and their dependence on the capture time constants can be visualized [Kan 1992b].

Let n_3 be the small signal carrier density in the SCH region and n_2 be the density of carriers in the confined states of QW. The small-signal rate equation describing the transfer of carriers into and out from QW is [Rideout 1991]:

$$\frac{dn_3}{dt} = \frac{i_{inj}}{qAw} - \frac{n_3}{\tau_3} - \frac{i_{net}}{qAw} \tag{19}$$

where q is the electronic charge, A is the junction area, w is the quantum well width, and τ_3 is the spontaneous lifetime. It is assumed that carriers in the SCH region are fed directly by an external injection current i_{inj}. The net current flowing into the QW (denoted by i_{net}) is the difference between the quantum capture and escape currents, $n_3(qAw)/\tau_{cap} - n_2(qAw)/\tau_{esc}$, where τ_{cap}, τ_{esc} are the capture and escape time constants, respectively [Rideout 1991].

The external voltage across the device (neglecting parasitics) is given by the difference of the quasi-Fermi levels in the SCH region ($V_3 = E_f^c - E_f^v$), which is related to the density of unconfined carriers. The small-signal relationship can be written as: $n_3(qAw_s) = c_3 v_3$ where w_s is the width of the SCH region, v_3 is the small-signal of V_3, and c_3 is the small-signal inversion capacitance associated with the unconfined carriers [Katz 1981, Harder 1982c]. Similarly, the

change of voltage across the quantum well is given by the difference of the quasi-Fermi levels in the quantum well, i.e., $V_2 = E_f^c(QW) - E_f^v(QW)$, which is related to the density of confined carriers: $n_2(qAw) = c_2 v_2$ where v_2 is the small-signal of V_2 and c_2 is the inversion capacitance associated with the confined carriers in QW [Harder 1990]. The expressions for c_2 and c_3 are given in [Harder 1982c, 1990]. Using these relations between carrier densities and voltages, we can rewrite Eqn.1 as:

$$i_{inj} = c_3 \frac{dv_3}{dt} + \frac{v_3}{r_3} + (\frac{v_3}{r_{cap}} - \frac{v_2}{r_{esc}}) \tag{20}$$

where $r_3 = \tau_3/c_3$, $r_{cap} = \tau_{cap}/c_3$, and $r_{esc} = \tau_{esc}/c_2$. Note that v_3 is the actual ac voltage on the device. The net current ($i_{net} = v_3/r_{cap} - v_2/r_{esc}$) flowing into the QW can be expressed as the current flowing between two nodes in a circuit by making the following transformation:

$$i_{net} = \frac{v_3 - v_2(\frac{r_{cap}}{r_{esc}})}{r_{cap}} \tag{21}$$

The node voltage $v_2(r_{cap}/r_{esc})$ is denoted as $\tilde{v_2}$ and the ratio r_{cap}/r_{esc} as B.

The equivalent circuit can now be constructed by using the small-signal rate equations for the confined carriers in QW and the photons, and taking i_{net} as the effective injection current:

$$\frac{dn_2}{dt} = \frac{i_{net}}{qAw} - \frac{n_2}{\tau_2} - vg'S_o n_2 - vg_o(1 - \epsilon S_o)s \tag{22}$$

$$\frac{ds}{dt} = \Gamma v g' S_o n_2 + \Gamma v g_o (1 - \epsilon S_o)s + \Gamma\beta\frac{n_2}{\tau_2} - \frac{s}{\tau_p} \tag{23}$$

where τ_2 is the spontaneous lifetime, v_g is the group velocity of light, g_o is the optical gain at the bias point, g' is the differential gain, ϵ is the gain compression coefficient, S_o is the photon density at the bias point, Γ is the optical confinement factor, and β is spontaneous emission coupling factor. An equivalent circuit of the quantum well alone (without regard for the SCH region) can then be constructed using the standard procedure, resulting in an RLC resonance circuit (Fig.8a) whose impedance is given by:

$$\frac{1}{Z_{QW}(f)} = \frac{i_{net}}{v_2} = j2\pi f c_2 + \frac{1}{r_2} + \frac{1}{j2\pi f L + r_s} \tag{24}$$

By combining Eqn.24 with Eqn.20 and 21, the overall equivalent circuit of the device is shown in Fig.8b. The total impedance $Z_{int}(f)$ is given by:

$$\frac{1}{Z_{int}(f)} = j2\pi f c_3 + \frac{1}{r_3} + \frac{1}{r_{cap} + BZ_{QW}(f)} \tag{25}$$

Note that the a.c. optical output is proportional to the current flowing through the inductor, $i_L = v_g g_o(1 - \epsilon S_o)s(qAw)$.

We now consider several qualitative features of the equivalent circuit. First, when the capture time is infinitely long ($r_{cap} \rightarrow \infty$), the equivalent circuit becomes a simple RC circuit (Fig.9a) with a time constant $r_3 c_3 = \tau_3$ = the spontaneous lifetime, which is on the order of a few nanoseconds. This represents the situation in which the QW is effectively non-existent and the inversion capacitance c_3 is responsible for limiting the modulation response of an LED (emitting light in the SCH region) to well below 1 GHz. In another extreme where the carrier capture is infinitely fast ($r_{cap} \rightarrow 0$, $r_{esc} \rightarrow 0$) but B remains to be nonzero, the equivalent circuit reduces to a RLC circuit as shown in Fig.9b. In this case, the inversion capacitance (c_3) DOES NOT produce a low frequency roll-off as in the previous case, but is added to the inversion capacitance for confined carriers (c_2) and thus lowers the relaxation oscillation frequency ($\sim 1/\sqrt{(BL)C_{eff}}$) where $C_{eff} = c_3 + Bc_2$. It is clear from Fig.9b that even in the event of infinitely fast carrier capture, the relaxation oscillation frequency of a quantum well laser is affected by the inversion capacitance for unconfined carriers (c_3) and the capture/escape ratio $B = r_{cap}/r_{esc}$.

For the intermediate case where the capture time is finite, a simple circuit analysis shows that, at high bias power (in which case $L \rightarrow 0$), the inductor current i_L (which is proportional to the optical response) can be expressed as:

$$i_L = \frac{i_{inj}}{r_{cap}[j\omega c_3 + \frac{1}{r_3 // r_{cap}}](-\omega^2 L c_2 + j\omega\frac{L}{r_2} + 1)} \tag{26}$$

where "//" denotes a parallel combination of the circuit elements. There are thus two spectral features in the modulation response: (1) a RC roll off at angular frequency

$$\omega = \frac{1}{c_3(r_3 // r_{cap})} = \frac{1}{\tau_3} + \frac{1}{\tau_{cap}} \tag{27}$$

and (2) a resonance at $\omega_r = 1/\sqrt{Lc_2}$. This is shown schematically in Fig.9c. Note from Eqn.27 that the RC roll off is NOT simply due to the spontaneous lifetime τ_3 but is a parallel combination of the spontaneous lifetime and capture time. Since the general estimates of capture time are on the order of 1-40 ps [Morin 1991, Eisenstein 1991], the RC roll off is dominated by τ_{cap} at frequency $1/(2\pi\tau_{cap})$ which may or may not be higher than the relaxation oscillation frequency. A similar RC roll-off effect can also result from carrier diffusion across a wide SCH region [Nagarajan 1992].

The computed total impedance and the modulation response are plotted in Fig.10a-c for various choices of parameters as shown in the figure caption. Comparing the impedance plot in Fig.10a&b, we notice a drastic reduction of the relaxation oscillation peak when B is reduced from 0.6 to 0.006 by increasing τ_{esc}. This is due to the reduction of the effect of v_2 by a factor of B ($\widetilde{v_2} = Bv_2$) in the complete equivalent circuit. The physical meaning is that: when τ_{esc} is long, the effect of relaxation oscillation inside the QW cannot be fed back to the SCH region. This result suggests that the ratio B can be estimated from the impedance measurement with parasitic contributions being eliminated. A long τ_{esc} also leads to less damping in QW lasers [Rideout 1991] as can be seen in modulation response plotted in Fig.10a&b. Fig.10c illustrate the case of long capture time which shows a RC roll-off and resonance peak as mentioned above.

Reference

Blom P.W.M., R.F. Mols, J.E.M. Haverkort, M.R. Leys and J.H. Wolter, Superlattices and Microstructures, 7, 319 (1990)

Bowers J.E., Solid State Electron., **30**, 129 (1987)

Brum J.A. and G. Bastard, Phys. Rev. **B**, **34**, 2500 (1986)

Eisenstein G., J.M. Wiesenfeld, M. Wegener, G. Sucha, D.S. Chemla, S. Weiss, G. Raybon and U. Koren, Appl. Phys. Lett., **58**, 158 (1991)

Harder C., J. Quantum Electron., **QE-18**, 333 (1982).

Harder Ch., B.J. Van Zeghbroeck, M.P. Kesler, H.P. Meier, P. Vettiger, D.J. Webb and P. Wolf, IBM J. Res. Develop., **34**, 568 (1990)

Kan S.C., D. Vassilovski, T.C. Wu and K.Y. Lau, IEEE Photon. Tech. Lett., 1992a

Kan S.C. and K.Y. Lau, IEEE Photon. Tech. Lett., (1992)

Katz J., S. Margalit, Ch. Harder, D. Wilt and A. Yariv, IEEE J. Quant. Electron., **QE-17**, 4 (1981)

Kesler M.P. and E.P. Ippen, Appl. Phys. Lett., **51**, 1765 (1987)

Lange C.H. and C.B. Su, Appl. Phys. Lett., **55**, 1704 (1989)

Lester L.F., S.D. Offsey, B.K. Ridley, W.J. Schaff, B.A. Foreman and L.F. Eastman, Appl. Phys. Lett., **59**, 1162 (1991)

Mittelstein M., Y. Arakawa, A. Larsson and A. Yariv, Appl. Phys. Lett., **49**, 1689 (1986).

Morin S., B. Deveaud, R. Clerot, K. Fujiwara and K. Mitsunaga, IEEE J. Quant. Electron., **QE-27**, 1669 (1991)

Nagarajan et al. (1992)

Nagarajan R., T. Fukushima, S.W. Corzine and J.E. Bowers, Appl. Phys. Lett., **59**, 1835 (1991)

Rideout W., W.F. Sharfin, E.S. Koteles, M.O. Vassell and B. Elman, IEEE Photon. Tech. Lett., **3**, 784 (1991)

Shaffin W.F., J. Schlafer, W. Rideout, B. Elman, R.B. Lauer, J. LaCourse and F.D. Crawford, IEEE Photon. Tech. Lett., **3**, 193 (1991)

Shimizu J., H. Yamada, S. Murata, A. Tomita, M. Kitamura and A. Suzuki, IEEE Photon. Tech. Lett., **3**, 773 (1991)

Su C.B. , Appl. Phys. Lett., **53**, 950 (1988)

Takahashi T. and Y. Arakawa, IEEE J. Quantum. Electron., **QE-27**, 1824 (1991)

Tucker R.S., J. Lightwave Tech., **LT-3**, 1180 (1985)

Uomi K., T. Mishima and N. Chinone, Appl. Phys. Lett., **51**, 78 (1985).

Wu T.C., S.C. Kan, D. Vassilovski, K.Y. Lau, C.E. Zah, B. Pathak and T.P. Lee, Appl. Phys. Lett., (1992)

Zhao B., T.R. Chen and A. Yariv, Appl. Phys. Lett., **60**, 313 (1992)

Table II

Calculated values of τ_{cap} and R for different structural parameters. The value of ΔE_f when $J_{net} \simeq 2000 A/cm^2$ is denoted by $(\Delta E_f)_{2000}$.

N_C ($10^{12}cm^{-2}$)	R	τ_{cap} (ps)	$(\Delta E_f)_{2000}$ (meV)
Vb = 0.2 eV			
2	0.003	3.0	85
3	0.013	3.1	45
4	0.054	3.3	18
5	0.19	3.6	7
6	0.48	4.0	4
Vb = 0.1 eV			
2	0.15	3.6	10
3	0.43	4.0	5
4	0.79	4.2	3
5	1.12	4.3	2
6	1.39	4.3	1

Figure Captions

Fig. 1.

Schematic illustration of the "reservoir" model.

Fig. 2.

Plot of $(dg/dn)_{eff}$ vs. threshold gain using data in Table I. Solid circles indicate lasing in the first quantized state; crosses indicate lasing in the second quantized state. Inset: the separate confinement heterostructure of the InGaAs tensile-strained single QW laser where λ_g and d for the regions A, B and C are respectively, 1.0 μm and 145nm, 1.1 μm and 145nm, 1.2 μm and 10nm, and region D is the $In_{0.41}Ga_{0.59}As$ quantum well.

Fig. 3.

Plot of $K'(= K - 4\pi^2\tau_p)$ vs. threshold gain using data in Table I.

Fig. 4

Plot of ϵ vs. $(dg/dn)_{eff}$ using data in Table I. The straight line is a least square linear regression fit of the data.

Fig. 5

Carrier capture process in QW structures. The parabolic sub-band associated with each longitudinal energy (E_z^c or E_z^u) is due to the transverse energy of the electron $(\hbar k_{//}^{(c,u)})^2/2m^*$.

Fig. 6

Various current components in a QW structure with $V_b = 0.15eV$ and $N_c = 4 \times 10^{-12}cm^{-2}$ at T=300K and the ratio R are plotted against ΔE_f.

Fig. 7

The ratio R vs. well thickness of $Al_{0.3}Ga_{0.7}As/GaAs$ QW for N_c = 2, 3, and $4 \times 10^{12}cm^{-2}$.

Fig. 8

(a) Equivalent circuit of photon-carrier interaction in QW; (b) Complete intrinsic equivalent circuit of quantum well laser.

Fig. 9

Equivalent circuit and schematic modulation response in the cases: (a) long capture time; (b) short capture time with finite B; and (c) intermediate case and high output power. (n_3 is the carrier density in SCH region and i_L is the inductor current which is proportional to the laser output.)

Fig. 10

Intrinsic impedance (left) and modulation response (right) in cases: (a) $\tau_{cap} = 5ps$, $\tau_{esc} = 5ps$, and B=0.6; (b) $\tau_{cap} = 5ps$, $\tau_{esc} = 500ps$, and B=0.006; (c) $\tau_{cap} = 50ps$, $\tau_{esc} = 50ps$, and B=0.5. The parameters used for calculation are: $\tau_2 = \tau_3 = 1ns$, $\tau_p = 2ps$, $A = 200\mu m \times 3\mu m$, $\beta = 10^{-4}$, $\epsilon = 10^{-17}cm^3$, $g' = 6 \times 10^{-16}cm^2$, and $\Gamma = 0.03$. In each case, three curves are plotted, corresponding to three different current levels, I=1.2 I_{th}, 4 I_{th}, and 20 I_{th} where I_{th} is the threshold current.

Transport Model

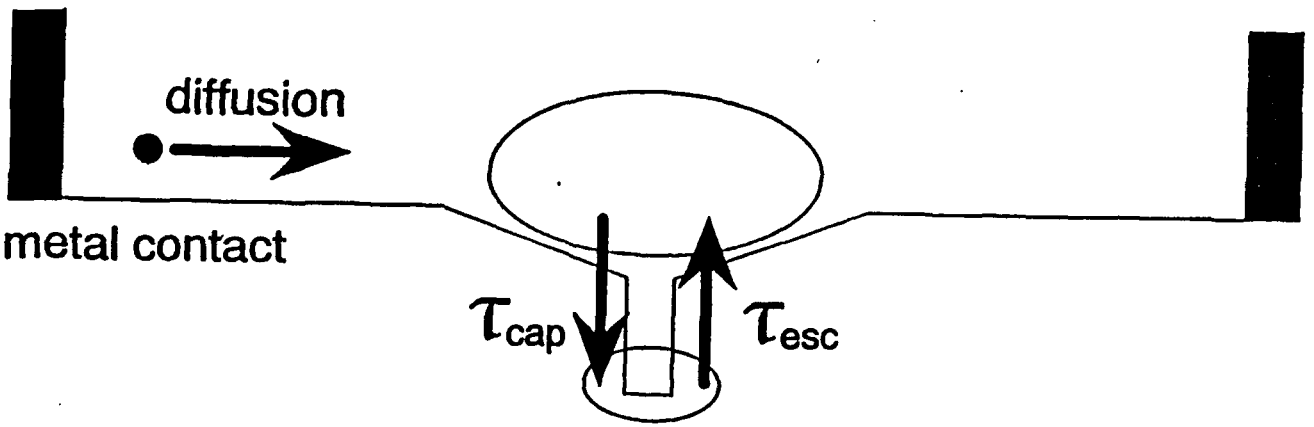

Fig 1

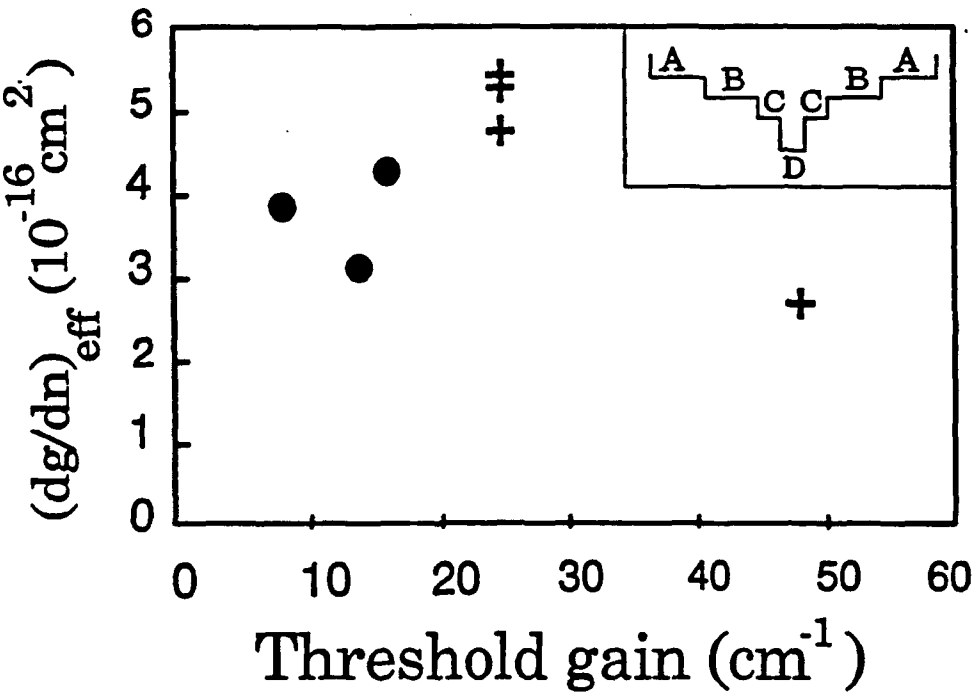
6
5
4
3
2
1
0
$(dg/dn)_{eff}$ $(10^{-16} cm^2)$
A
B
C
C
B
A
D
0
10
20
30
40
50
60
Threshold gain (cm^{-1})

Fig. 2

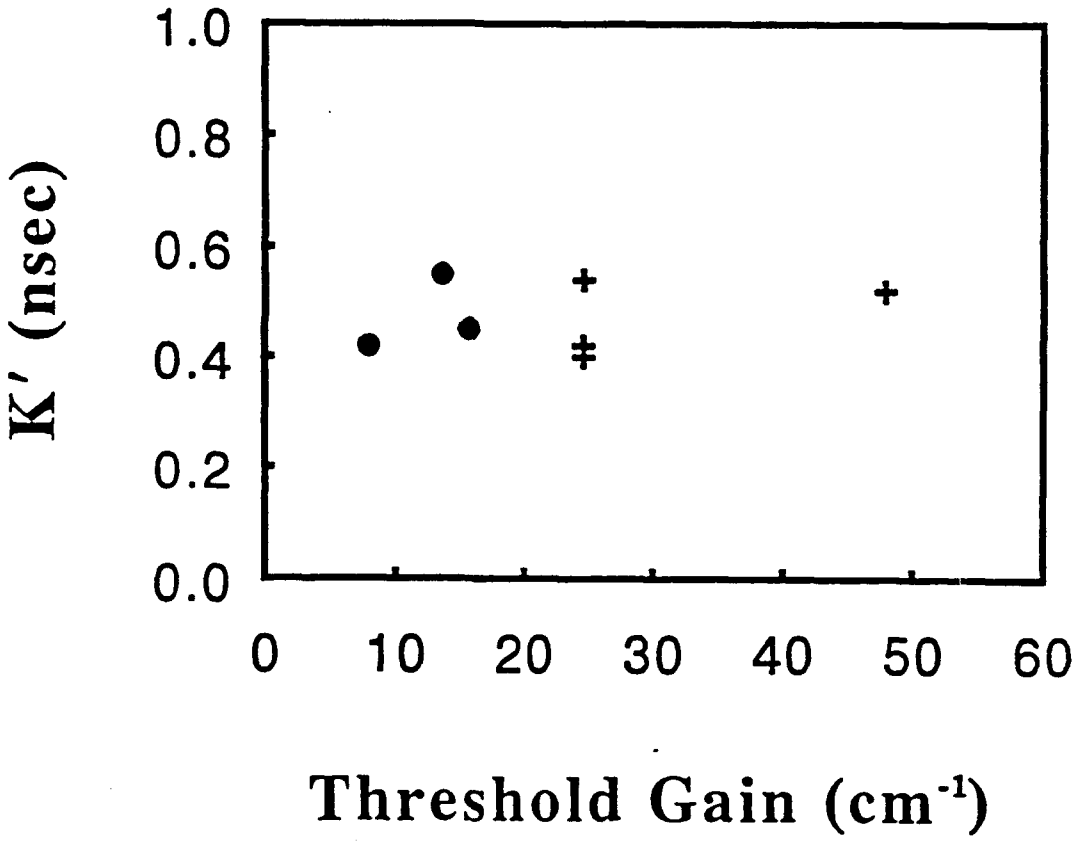

Fig 3

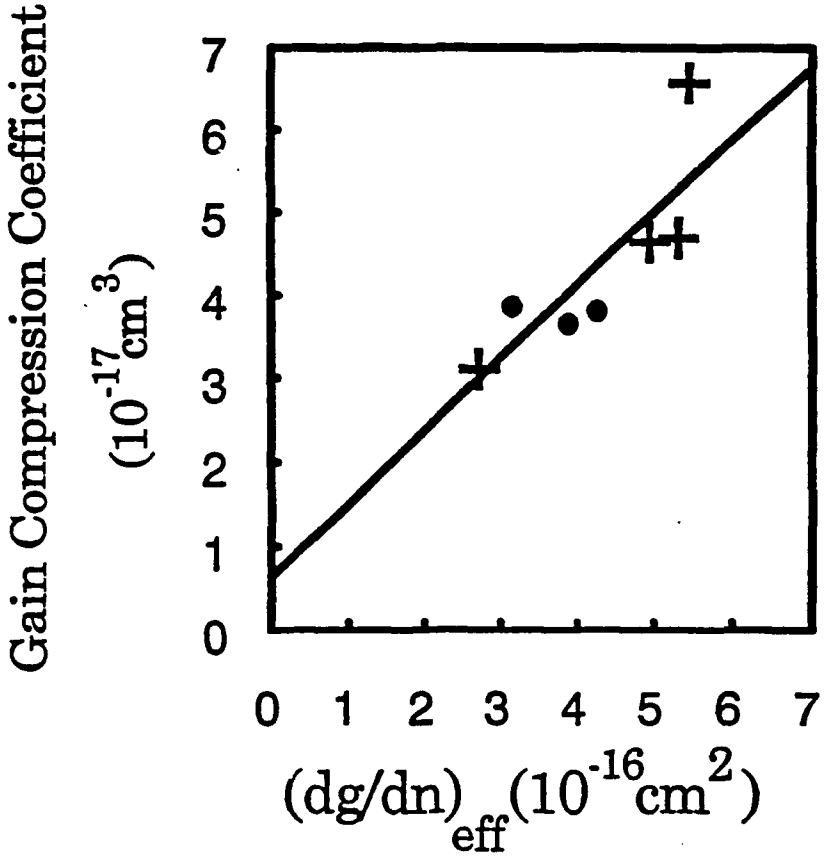
Gain Compression Coefficient
$(10^{-17}cm^3)$
0
1
2
3
4
5
6
7
0 1 2 3 4 5 6 7
$(dg/dn)_{eff}(10^{-16}cm^2)$

Fig. 4

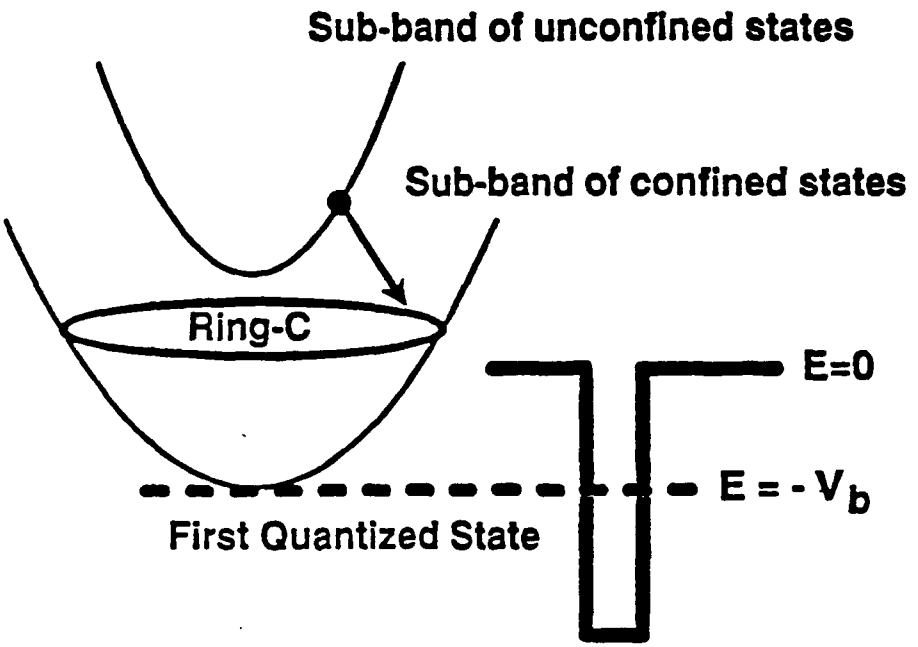
Sub-band of unconfined states
Sub-band of confined states
Ring-C
E=0
E = - V_b
First Quantized State

Fig. 5

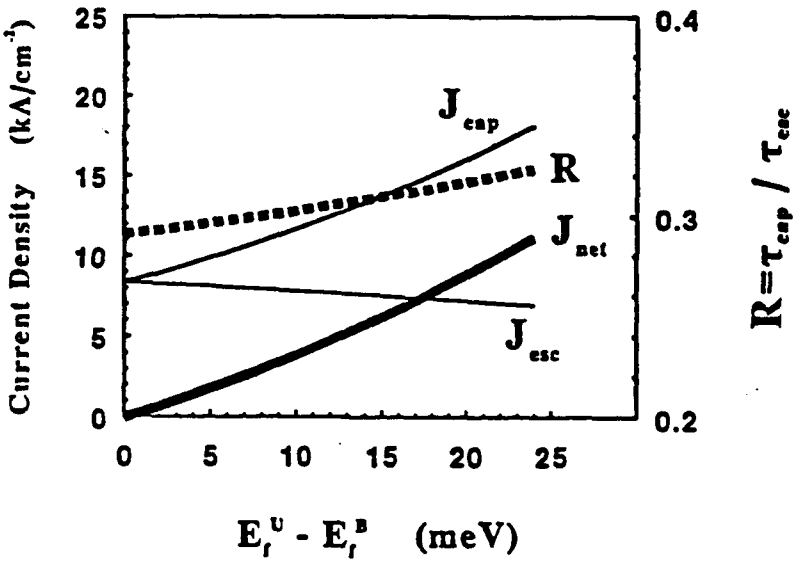
Current Density (kA/cm²)
25
20
15
10
5
0
0.4
0.3
0.2
R=τcap / τesc
Jcap
R
Jnet
Jesc
0
5
10
15
20
25
E_f^U - E_f^B (meV)

Fig. 6

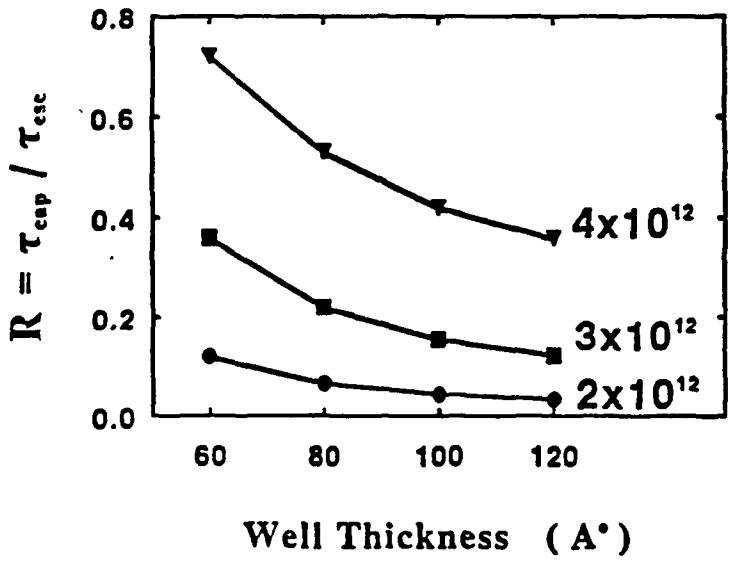
0.8
0.6
0.4
0.2
0.0
R = τcap / τesc
4x10^12
3x10^12
2x10^12
60
80
100
120
Well Thickness (A°)

Fig.7

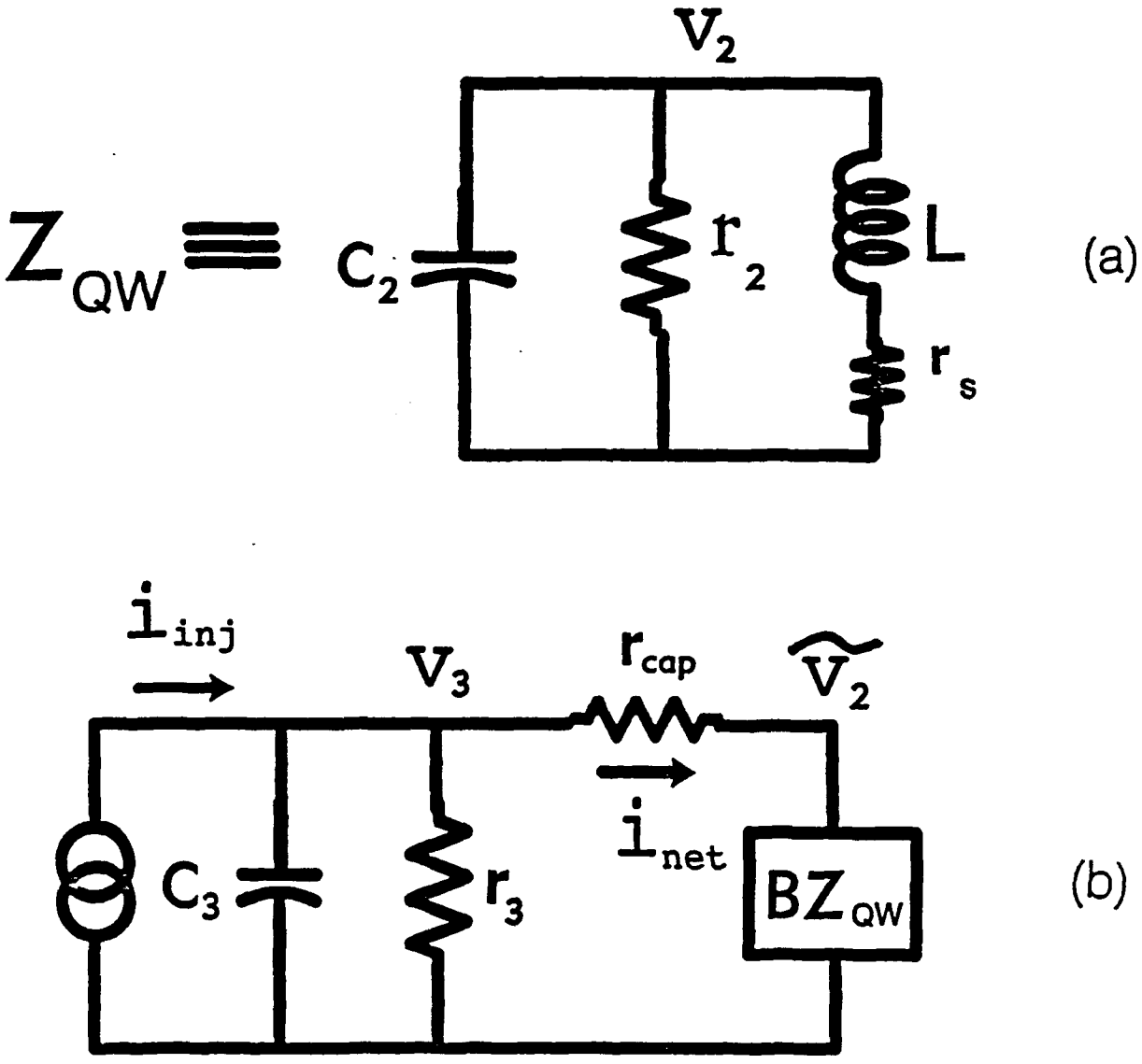

Fig. 8

(12)

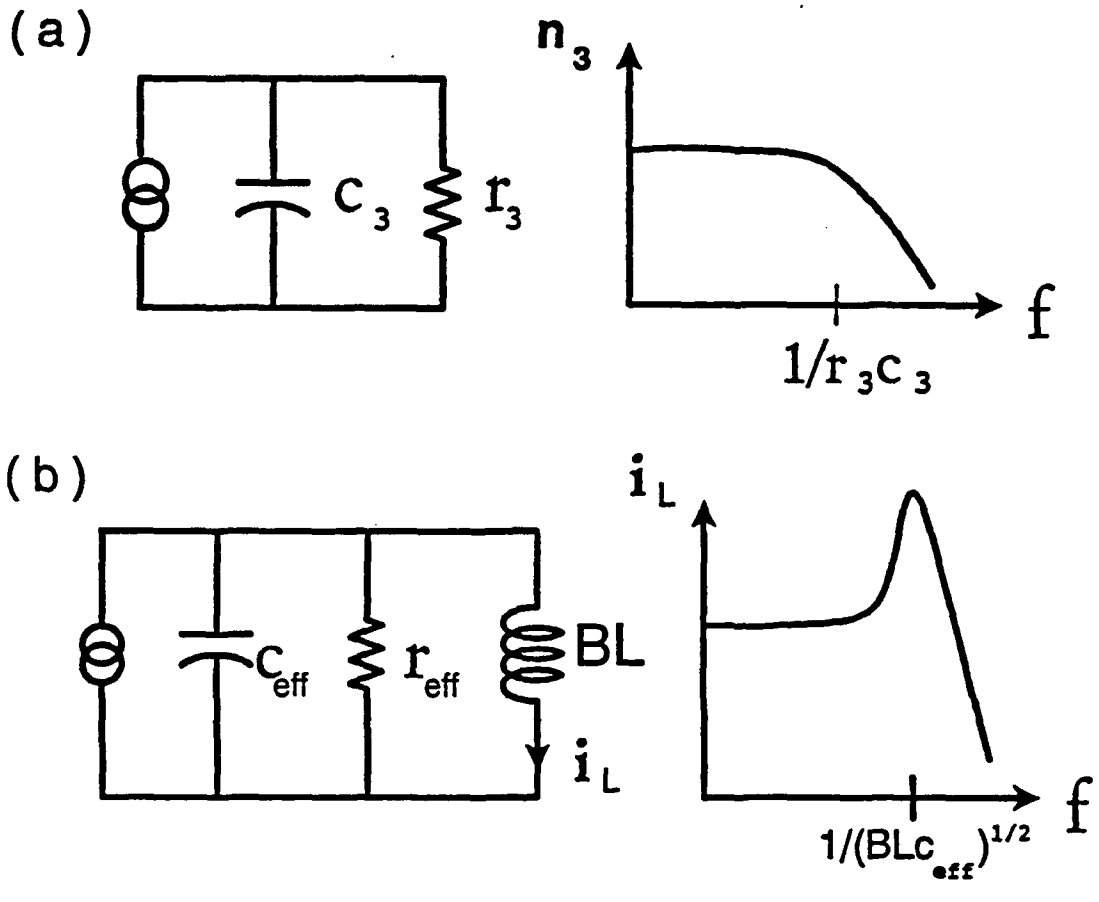
(a)
n_3
C_3
r_3
f
$1/r_3c_3$
(b)
i_L
C_{eff}
r_{eff}
BL
i_L
f
$1/(BLc_{eff})^{1/2}$
(c)
i_L
f
$\frac{1}{(r_3 // r_{cap})c_3}$
$\frac{1}{(Lc_2)^{1/2}}$

Fig. 9

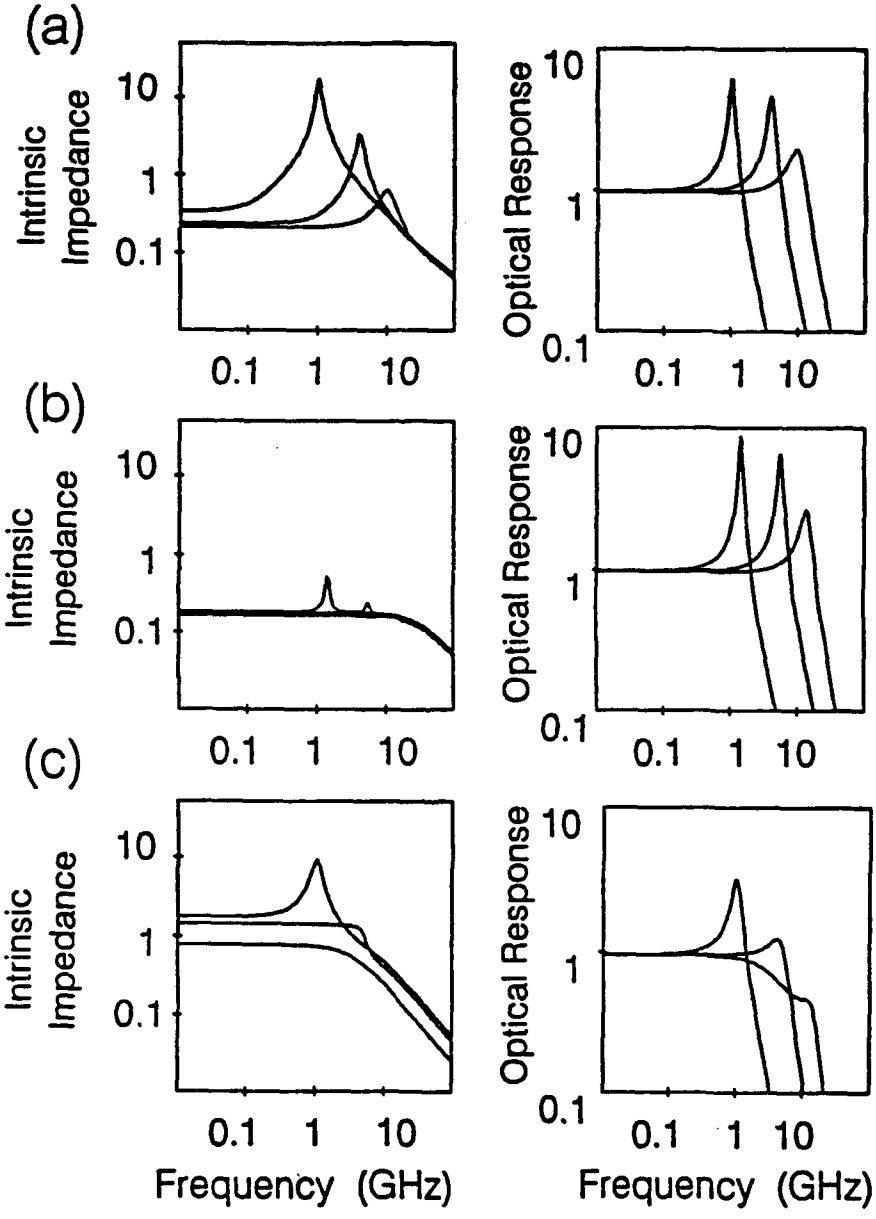
(a)
(b)
(c)
Intrinsic Impedance
Optical Response
10
1
0.1
0.1
1
10
Frequency (GHz)

Fig. 10